Polymer-Coated Radioluminescent Nanoparticles for Quantitative Imaging of Drug Delivery

*Thomas L. Moore, Fenglin Wang, Hongyu Chen, Stuart W. Grimes, Jeffrey N. Anker, and Frank Alexis**

Some theranostic nanoparticle (NP) drug delivery systems are capable of measuring drug release rates in situ. This can provide quantitative information regarding drug biodistribution, and drug dose that is delivered to cells or tissues. Here, X-ray excited optical luminescent (XEOL) NPs coated with poly(glycolide)-poly(ethylene glycol) (XGP) are used measure the amount of drug released into cells. The photoactive drug protoporphyrin IX (PpIX) is loaded into XGP and is able to attenuate the XEOL NP emission. Measuring an increase in XEOL intensity as PpIX is released enables the measurement of drug release into glioblastoma cells (GBM). Biodistribution studies in a BALB/c mouse GBM intracranial xenograft model show significant XGP accumulation at the site of the GBM xenograft within the brain, and not in adjacent healthy brain tissues. There is no uptake of XGP in the heart or kidneys, the primary organs associated with drug and gadolinium ion toxicity. NP toxicity is tested with U-138MG GBM in vitro, and NPs show low cytotoxicity at concentrations of 100 µg/mL. In vivo dose escalation studies in BALB/c mice show no adverse effects at doses up to 75 mg/kg. These theranostic NPs offer an approach to quantitatively measure drug release into cells.

1. Introduction

Theranostic nanomedicine is an emerging field in which nanoparticles (NPs) are able to mediate both diagnosis and therapy.[1] Theranostic approaches are expected to provide real-time feedback of drug biodistribution or drug concentration, which may indicate the therapeutic efficacy. The purpose of early theranostic NP systems, which combined drug delivery with imaging, was to non-invasively show the co-localization of drug and delivery vehicle at the disease site.[2] However, the next generation of theranostic NPs are able to non-invasively and quantitatively report in situ drug doses.[3–6] Such systems could improve understanding of the delivered drug dose into cells and tissues. Since drugs are ineffective until they are released from the NPs, a quantitative theranostic approach could provide a better indication regarding the amount of drug delivered to the tumor by differentiating between drug loaded within the NPs and drug that has been released. Theranostic NPs may also be useful in non-invasively determining the intracellular drug delivery to establish the amount of drug delivered into the cells, which is difficult to determine with conventional in vitro drug release kinetic studies. This use of theranostic NPs is critical because neither *in vitro* studies nor animal studies can accurately predict the release kinetics into cells or tissues. Nor can they predict the drug distribution into a heterogeneous tumor.

While NP drug delivery systems exhibit a therapeutic effect against glioblastoma cells (GBM) in vitro and in vivo, little is known about the release kinetics and drug doses delivered into the cells and tumors. If the drugs are released too rapidly, NPs cannot carry them to the tumor; if the drugs are released too slowly, they can lose their efficacy. Also, current methods to monitor the progress of GBM cannot provide immediate feedback as to how and where drugs are released to make distinctions of drug doses. Complicating these difficulties are the high interstitial fluid pressure, variable intratumoral pH, irregular vascular hierarchy, and variable extracellular matrix in the tumor microenvironment that prevents effective drug delivery into tumors.[7] These pathophysiological differences may in turn result in differences in either the release kinetics (e.g. due to variation in pH) or may result in a lower intratumoral accumulation of NPs (e.g. variance in the EPR effect), and ultimately result in variable intratumoral drug concentrations.[8] Thus, there is a growing need for robust theranostic NPs that are capable of non-invasively measuring the drug doses and release kinetics in tumor cells.

X-ray excited optical luminescence (XEOL), or radioluminescence, is a phenomenon whereby X-ray is converted into visible light. As X-rays possess excellent soft tissue penetration, XEOL offers an appealing approach for use as an imaging modality. XEOL provides deep tissue penetration, and avoids tissue autofluorescence.[9–11] Through a combination of luminescent imaging at multiple angles and/or multiple X-ray excitation

Dr. T. L. Moore, S. W. Grimes, Prof. F. Alexis
Department of Bioengineering
Clemson University
301 Rhodes Research Center
Clemson, SC 29634, USA
E-mail: falexis@clemson.edu
F. Wang, Dr. H. Chen, Prof. J. N. Anker
Department of Chemistry
Center for Optical Materials Science and Engineering Technology (COMSET)
118 Biosystems Research Complex
Clemson, SC 29634, USA

DOI: 10.1002/adfm.201400949

patterns, one can construct the 3D distribution of NPs in the tissue using a technique known as X-ray luminescence tomography (XLT).[5,10–16] High resolution images can be acquired, limited by the X-ray beam width in the tissue, by scanning a pencil-shaped X-ray beam through the tissue and acquiring single pixel measurements at each point.[10,15,16] Alternatively, more rapid analysis is possible by using information in the optical luminescence image analysis.[5,11,12] While the quickest analytical technique entails the use of a single pencil-shaped beam for low background luminescence tomography, it is possible to achieve higher resolution using a scanning fan or cone-shaped beam. The tomography can be enhanced by the co-registered information from either the X-ray transmittance images or the CT scan.

Similarly, photoluminescent NPs have been investigated as a means for measuring the in situ release kinetics of doxorubicin, ibuprofen, or photoactivated drugs. While numerous studies do indicate the utility of either fluorescent or upconversion NPs for measuring drug release,[4,6,17,18] very few of these studies have used radioluminescent NPs.[5] In this paper, we describe the development of polymer coated radioluminescent NPs for the controlled release of the photo-absorbent and phodynamic drug, protoporphyrin IX (PpIX), which is currently used clinically in photodynamic therapy (PDT).[19] One advantage of using these photoactive drugs such as PpIX, as compared to doxorubicin and other chemotherapeutic agents, is that the direct application of light must be used to activate the drug (~635 nm). PpIX is traditionally administered as a prodrug 5-aminolevulinic acid, which is biosynthetically converted into PpIX in vivo. Though the doses of photosensitizers and light in PDT used to treat GBMs did vary in clinical trials, the median survival for a primary GBM multiform (WHO grade IV) was prolonged from 15 to 22 months, and for recurrent GBM from three to nine months. Surgery and light activation is regularly undertaken in cancer treatments even though the dose of the photosensitizer in the tumor is unknown. Knowing this exact dosage to the tumor is critical in determining the therapeutic efficacy of the PDT in GBM multiform patients, because the efficacy depends upon the accumulation of the drug into the tumor and the total amount of intracellularly synthesized PpIX in tumor cells.[20] Controlling PpIX accumulation and release is important because in vivo it is degraded to heme and cleared within 24–48 h.[21] In experiments in which PpIX was incorporated into a pH-sensitive NP drug delivery system comprised of poly(β-amino ester)-poly(ethylene glycol) micelles, in vitro fluorescence measurements showed a pH-dependent release of PpIX over a 72 h period with 60% of the drug released in the first 24 h at pH 6.4.[22] However, this fluorescent approach would be difficult in situ, and significant challenges remain to measure drug release kinetics into cells and tissues.[23]

In this work, we coated spherical Gd_2O_2S:Eu NPs with poly(glycolide)-poly(ethylene glycol) (PGA-PEG) to encapsulate PpIX into the polymer shell to both prolong its release through diffusion, and to measure the intracellular release using XEOL. When loaded with PpIX, the XEOL emission of Gd_2O_2S:Eu at 625 nm overlaps with the optical absorbance of PpIX at 630 nm, and this reduced the Gd_2O_2S:Eu-PGA-PEG NPs (XGP) radioluminescent signal at 625 nm when compared to the signal at 700 nm. Thus, measuring the peak ratio at 625 and 700 nm of XGP showed a dose dependent relationship between the amounts of loaded PpIX. Our release studies of the PpIX-loaded XGP indicated that the radioluminescence detected the PpIX release in PBS. We determined that the XEOL signal strength of the XGP increased with the release of the PpIX. We also measured the intracellular release kinetics in vitro in U-138MG GBM cells. In our biodistribution studies, we injected XGP into the tail veins of athymic BALB/c mice bearing intracranial U-138MG GBM xenografts. Our subsequent radioluminescent imaging showed an accumulation of XGP in the brain tumor, spleen, liver, and lungs. Finally, we observed no significant adverse effects associated with both the coated and uncoated Gd_2O_2S:Eu NPs at concentrations up to 100 μg/mL in U-138MG cells in vitro, and in BALB/c mice after injections up to 75 mg/kg.

2. Results and Discussion

2.1. Nanoparticle Synthesis & Characterization

Gadolinium oxysulfide-based X-ray luminescent NPs (Gd_2O_2S:Eu NPs) were synthesized because they are excited by deeply penetrating X-rays, emit in the red region, with only a minimal emission of autofluorescence from the tissue. These nanophosphors are also useful for fluorescence microscopy due to the narrow excitation and emission peaks, excellent photostability, and low toxicity.[5,13,15,24] The spherical radioluminescent NPs, which were approximately 40 nm in diameter, were synthesized via precipitation of a $Gd_2O(CO_3)_2{\bullet}H_2O$ precursor, doping with NaF, the addition of an additional $Gd_2O(CO_3)_2{\bullet}H_2O$ protective layer to prevent aggregation, finally followed by calcination at 600 °C and sulfidation at 700 °C. Electron-hole pairs are generated in the host lattice under X-ray excitation, and these electron-hole pairs then excite Eu^{3+} centers which emit visible and near infrared light.

This theranostic approach required the use of an optically absorbent drug (PpIX), which absorbed light at wavelengths corresponding to the luminescent emission spectrum of the radioluminescent XGP. **Figure 1** shows a schematic representation of this treatment paradigm. The Gd_2O_2S:Eu NPs were excited by X-ray radiation after coating with an amphiphilic polymer (PGA-PEG). When the PGA coating was loaded with a hydrophobic PpIX via encapsulation, the absorption of light by the PpIX in the particles and nearby solution quenched the radioluminescence emission of Gd_2O_2S:Eu at 630 nm. The hydrophobic drug was then released by diffusion and degradation of the biodegradable polymer layer. As drug was released and removed or degraded, luminescent intensity increased due to the relative absence of drug molecules needed to quench the radioluminescent signal.

Gd_2O_2S:Eu NPs were functionalized with amine groups, which served as the initiation site for the polymerization of PGA. A room temperature, bottom-up, surface initiated ring-opening polymerization was used to grow PGA directly from the inorganic nanoparticle surface. Subsequent thermogravimetric analysis (TGA) showed a PGA coating of approximately 20 wt%. PEG was conjugated to the PGA chain ends via isocyanate chemistry. Methoxy-poly(ethylene glycol)-isocyanate was

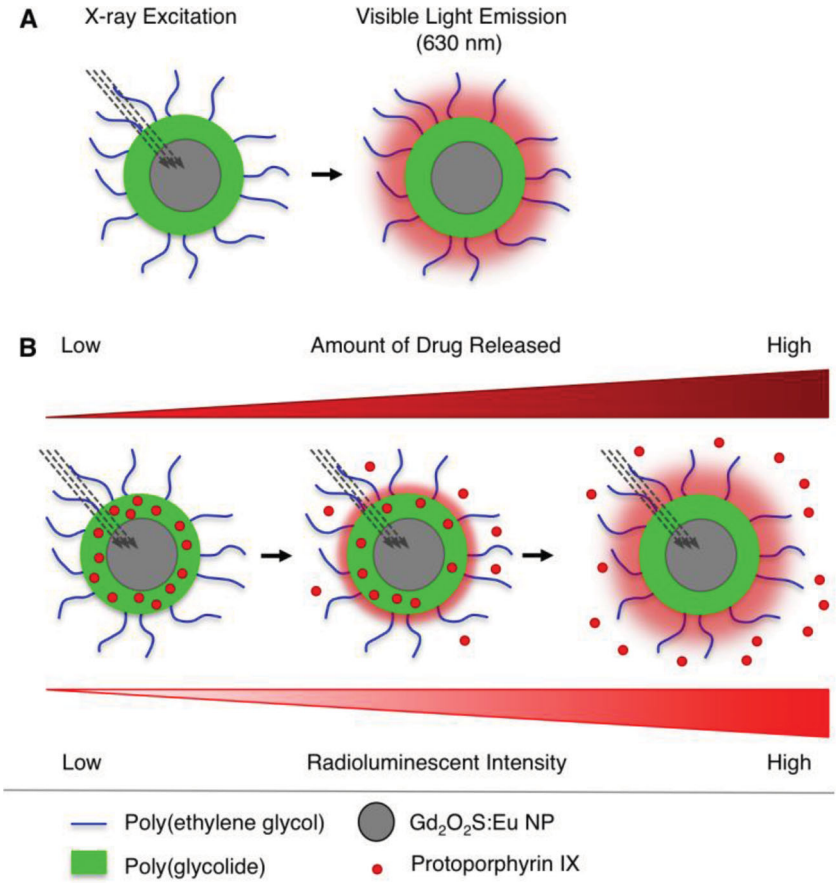

Figure 1. (A) Radioluminescent NPDDS was composed of a Gd_2O_2S:Eu core, and a polyglycolide-poly(ethylene glycol) (PGA-PEG) coating. X-ray radiation was used to excite the inorganic core with a visible light emission at 625 nm. (B) The hydrophobic photosensitizer, protoporphyrin IX (PpIX), was loaded within the hydrophobic PGA matrix. PpIX, when loaded into the PGA shell, reduced the radioluminescent signal from Gd_2O_2S:Eu. The release of the drug enhanced the relative luminescent intensity which was measured to quantify the amount of the drug released.

added directly into the reaction containing Gd_2O_2S:Eu-PGA NPs, which resulted in the isocyanate groups reacting with the terminal hydroxyl groups on the PGA chain ends. The final product was a radioluminescent NPs with a PGA-PEG shell (XGP), and TGA data showed a PEG coating of 10 wt% (**Figure 2**A). The final product was also characterized via Fourier transform infrared spectroscopy (Figure 2B). Photographs of uncoated Gd_2O_2S:Eu NPs and XGP under white light and X-ray irradiation indicated that the XEOL of the inorganic Gd_2O_2S:Eu NP core was maintained after coating (Figure 2C). Finally, transmission electron microscopy (TEM) of both the uncoated NPs and XGP indicated evidence of a polymeric coating (inset images).

2.2. Nanoparticles to Measure Drug Loading

We also determined the feasibility of using XGP to measure both the drug loading and the release kinetics. Although PpIX was used in this study, it is possible to use other drugs by tuning the emission wavelength of the radioluminescent NPs.[4,5,18] **Figure 3**A shows the optical profile of PpIX and the absorption maxima: at 500, 540, 570, and 630 nm, respectively. An overlay of the photoluminescent emission spectrum of XGP under X-ray excitation clearly shows a peak overlap at 625 nm, which allows for the quantitative measuring of the PpIX loaded within the XGP. PpIX was loaded into XGP via encapsulation, and with various initial concentrations that resulted in a concentration-dependent reduction of the 625 nm XEOL. Figure 3B shows the X-ray luminescent spectrum of XGP when loaded at different concentrations of PpIX. The peak at 625 nm shows a distinct attenuation from the increased loading of the PpIX. The peak at 700 nm, however, is relatively unaffected, because PpIX lack a strong absorbance at the 700 nm wavelength. The peak ratio for XGP was calculated by averaging the peak intensity across the full-width (FW_{AVG}) at 625 nm, and normalizing by the FW_{AVG} intensity at 700 nm. This ratio provides an internal reference, and it is therefore possible to measure drug loading independent of the X-ray beam intensity. It is apparent that higher drug loading results in greater signal attenuation from the XGP samples (Figure 3C). This phenomenon was observed in both water, and after loading XGP and injecting into porcine muscle tissue (Figure 3D). Cubes of porcine muscle tissue were cut into ~2.5 cm^3 blocks and injected at 1 cm deep with XGP loaded with various concentrations with PpIX. This data illustrates the possibility of measuring, through thick tissue, different concentrations of XGP loaded with PpIX.

2.3. Luminescent Measurement of Release Kinetics

It was also possible to measure the release kinetics of PpIX from XGP (**Figure 4**). After loading with PpIX via encapsulation, XGP was incubated in a dialysis unit at 37 °C in PBS. At each time point, the radioluminescent intensity was measured for the XGP, and the release media was exchanged. Luminescent intensity measurements were reported as a ratio of the FW_{AVG} at 630 nm to the FW_{AVG} at 700 nm. These data were compared to fluorescent measurements made of free PpIX within the release media dialysate. As time progressed, the radioluminescent intensity of XGP increased, indicating less quenching from the release of the drug. Similarly, as time progressed the cumulative amount of free PpIX detected in the dialysate also increased, suggesting that in a controlled setting, the amount of PpIX either loaded or released could be detected based upon the radioluminescence of XGP. In order to study the intracellular release of PpIX in vitro with U-138MG, kinetic uptake studies of XGP in U-138MG were performed. Cells were incubated with XGP for 3, 6, and 24 h.

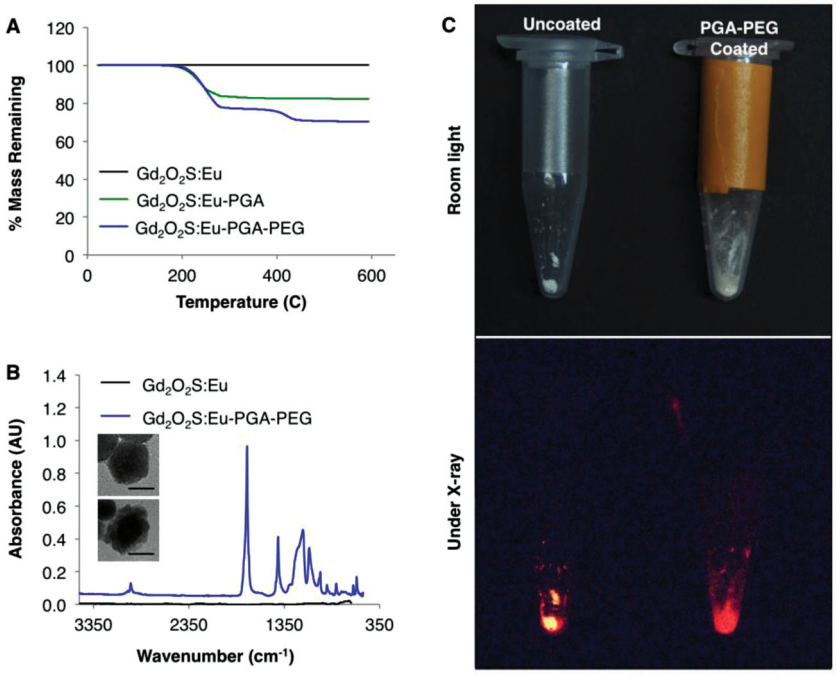

Figure 2. (A) Thermogravimetric analysis of the NPPDS indicated a 20 wt% coating of PGA, and 10 wt% of PEG. (B) Fourier transform infrared spectroscopy further confirmed a polymeric coating. The ester bond present in PGA from the carbonyl group is observable at 1745 cm^{-1}. Insets show TEM images of uncoated NPs (top), and PGA-PEG coated NPs (bottom). Scale bars represent 20 nm. (C) Photographs of uncoated and coated NPs under visible light (top), and under X-ray irradiation (bottom) in the dark show radioluminescence.

At each time point cells were gently washed twice with sterile PBS, trypsinized to remove NPs on the surface of cells, and radioluminescent images were taken with the IVIS small animal imaging system with the portable X-ray source. A subsequent region of interest (ROI) analysis of repeats in triplicate for each time point revealed a maximum radioluminescent intensity at 24 h, indicating this to be the maximum time point tested for the cellular uptake of XGP (Figure 4B). Kinetic release studies in vitro were performed by incubating PpIX-loaded XGP with U-138MG for 24 h, after which cells were washed gently with PBS. At each time point, the samples were then lysed using a freeze-thaw method.[25] Cell debris and XGP were pelleted via centrifugation, and radioluminescent measurements were taken. The supernatant containing released PpIX was analyzed using fluorescence. Figure 4D shows the radioluminescent measurements of the pellet containing cell debris and XGP (red). The fluorescent measurements (blue) of the supernatant from lysed cells showed that cumulative released PpIX content increased over time (Figure 4D). The XGP radioluminescence (red) also increased over time, which indicated a release of the drug. Next, cellular pellets were dissolved in an organic solvent to extract any of the drug remaining encapsulated within XGP, which was then further quantified via fluorescence (Figure 4E). This data showed a decrease in remaining drug encapsulated within XGP over time. A notable and significant difference between the release kinetics in PBS (Figure 4A) and intracellular release kinetics (Figure 4D) was also observed. Fluorescence measurements of total free PpIX measured from the cellular supernatant showed a 15-fold increase compared to the total drug released in PBS in 48 h. There was a 20% increase in the radioluminescent intensity for the intracellular release compared to release in PBS, demonstrating the effectiveness of using NP radioluminescence to measure the drug release kinetics. We also showed the inadequacy of using a simple PBS release system to attempt to model the kinetics in a cellular environment. The resulting accelerated release into

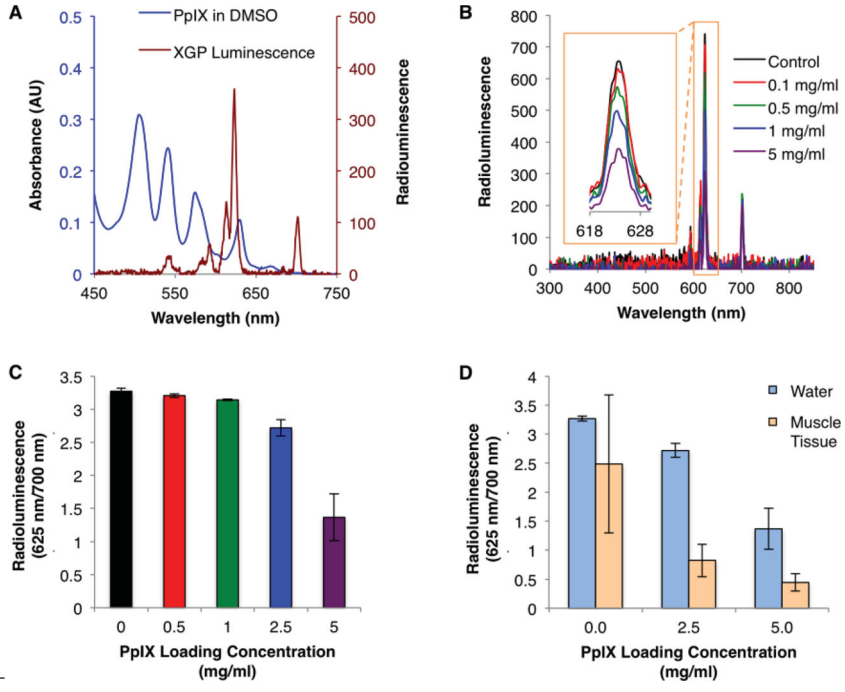

Figure 3. (A) The absorption spectrum of the PpIX overlaid with the radioluminescent spectrum of XGP. The absorbance peak of PpIX at 630 nm, and the emission peak of the XGP at 625 nm indicates that this combination is a viable pairing for a theranostic NPDDS. (B) Radioluminescence spectra of the XGP loaded with various concentrations of PpIX indicates a dose-dependent reduction of the XGP emission at 625 nm. (C) Comparing the radioluminescent signal intensity of the XGP loaded with PpIX to the XGP without the drug shows a relationship between the radioluminescent peak ratio to the amount of drug loaded. (D) Measuring these drug loading was possible in both water, and through porcine muscle tissue.

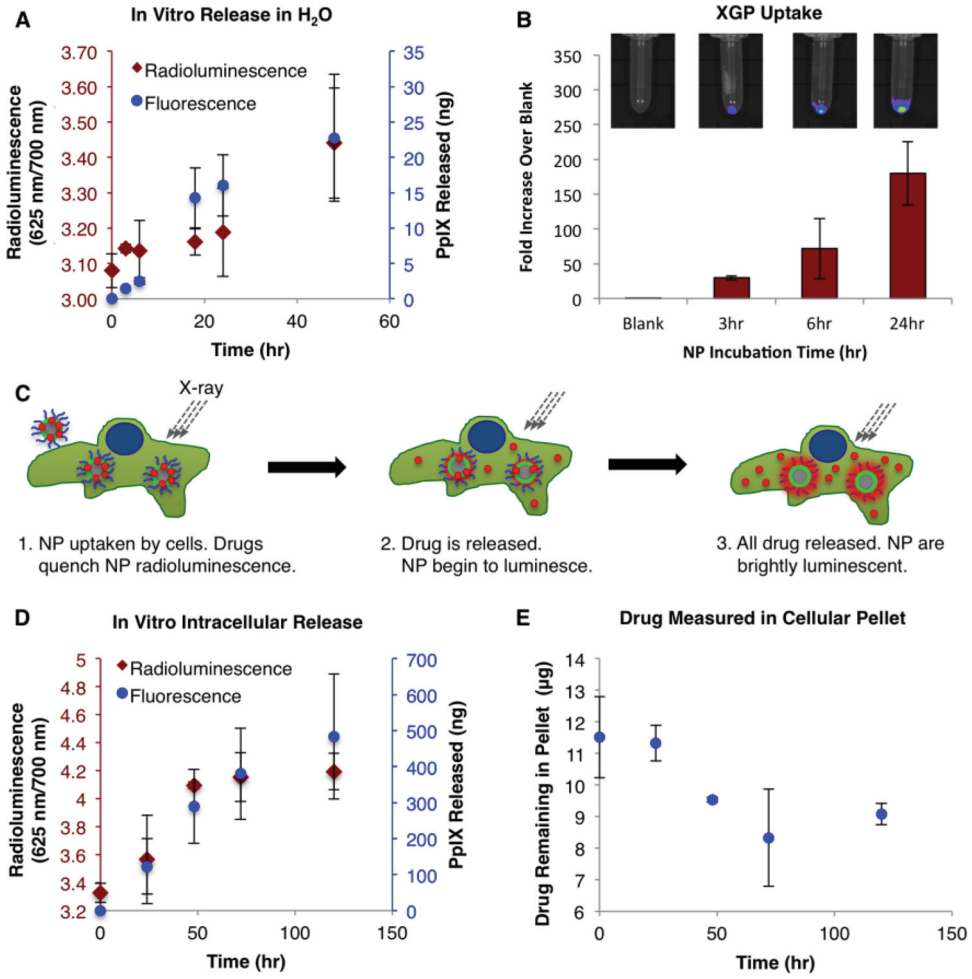

Figure 4. (A) Release kinetics of the PpIX from the XGP measured with XGP radioluminescence peak ratio (red), and fluorescence measurements of PpIX (blue) in release media dialysate. (B) Kinetic uptake study of XGP in U-138MG cells shows maximum NP uptake after 24 h. (C) Schematic representation of the intracellular release kinetics study. (D) Radioluminescent (red) measurements of U-138MG cellular pellets showed increasing intensity over time, which indicates a release of PpIX from XGP. Fluorescence measurements (blue) of the supernatant from lysed cells shows the cumulative amount of free, or released, PpIX. (E) Fluorescent measurement of PpIX measured within the cellular pellet indicates a decrease in the PpIX content loaded in the XGP over time.

the cells is perhaps due to either the acidic pH, or the enzyme activity degrading the polymer coating and increasing the diffusion of PpIX.[26] Clearly, these results demonstrate the critical importance of measuring the drug release kinetics into cells. Confocal microscopy also showed an intracellular delivery of the PpIX by XGP within U-138MG (**Figure 5**). Cells were incubated for 6 h with either cell culture media as a control, free PpIX, XGP without PpIX, or XGP loaded with PpIX. They were then stained for actin (green), and nuclei (blue), and the inherent PpIX fluorescence was also imaged (red). As expected, the control cell culture media, and U-138MG incubated with empty XGP (no drug) did not exhibit any fluorescence. Furthermore the U-138MG incubated with the free drug also did not show fluorescence, whereas the XGP with the PpIX did exhibit a fluorescent signal within the cells. This fluorescence suggests the necessity of using XGP to improve the uptake of PpIX, and deliver the drug intracellularly.

2.4. In Vivo Biodistribution

An investigation of the NP biodistribution using brain tumor xenografts in athymic BALB/c mice determined that it was possible to non-invasively image XGP accumulation into the GBM tumors. Here, mice were implanted with intracranial xenografts of U-138MG cells, and after 10 days of tumor growth XGP was administered systemically via tail vein injection. After injection (24 h), the mice were imaged in an IVIS Lumina XR live animal imaging system with a portable X-ray excitation source (**Figure 6**). The non-specific accumulation of XGP within the tumor was clearly observed. Following euthanasia, the organs were explanted and luminescent images were taken with X-ray excitation. Observations clearly indicated a significant NP accumulation at the site of the xenograft within the brain, indicating the passive accumulation of XGP within the tumor. There was also accumulation of XGP within the organs of the reticuloendothelial system (i.e. liver and spleen), as well as in the lungs.

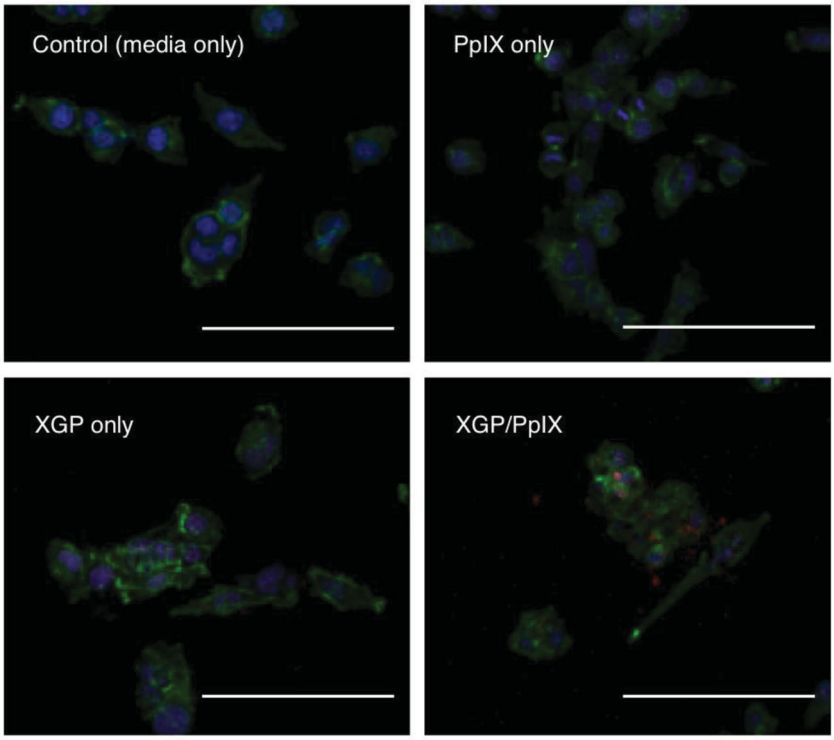

Figure 5. Confocal microscope images of U-138MG after incubation for 6 h with media only, PpIX only, XGP only, or XGP loaded with PpIX. Cells were stained for actin (green), cell nuclei (blue), and PpIX was imaged using fluorescence (red). Free PpIX was not detected within cells. When loaded within XGP, however, it was possible to detect PpIX localized in the cells. Scale bars represent 50 μm.

Importantly, there was no uptake of XGP in both the heart and the kidneys, the primary organs associated with drug and gadolinium (Gd) ion toxicity. Although the Gd-based MRI contrast agents are widely used (>200 million patients), they can cause nephrogenic systemic fibrosis (NSF) in patients with severe kidney disease, including many cancer patients undergoing chemotherapy.[27] The toxicity of Gd-based MRI contrast agents associated with the amount of Gd that dissociates from its chelate and deposits in the kidneys.

2.5. In Vitro and In Vivo Toxicity

An investigation of the in vitro toxicity of uncoated Gd_2O_2S:Eu NPs and XGP in U-138MG cells showed a toxicity of XGP at concentrations greater than 100 μg/mL. Cells were treated with various doses of either uncoated NPs or XGP for 24 h with, after which cell viability was quantified using a Presto Blue assay. Cells treated with only a cell culture media were used as a control, and samples were compared to the control using a Tukey's HSD test (**Figure 7**A). While in vitro cytotoxicity provides some information about the safety aspects of XPG, it also has numerous limitations including lack of hemostasis. Preliminary in vivo toxicity studies showed no adverse effects of XGP at doses up to 75 mg/kg in BALB/c mice (Figure 7B). Mice were injected with various doses of XGP and observed for behavioral signs of significant toxicity; a loss of 15% of initial body weight was classified as toxic. No sign of morbidity or weight loss was registered at a dose of 75 mg/kg (maximum dose tested). There are six FDA approved Gd-containing contrast agents used in MRI including Gadavist. Gadavist prefilled syringes are administered at a recommended dose for contrast imaging at 0.1 mL/kg body weight (60 mg/kg). Nanomaterial toxicity is generally dictated by NP size, shape, material, surface properties, degradation, and stability.[28] These in vivo data appear to be comparable with other studies of nanomaterial toxicity in vivo such as nano-hydroxyapatite,[29] gold nanoparticles,[30] or iron oxide.[31]

3. Conclusion

We presented multifunctional theranostic NPs comprising an XEOL NP core, and a PGA-PEG polymeric coating. X-rays were used to excite the inorganic Gd_2O_2S:Eu NPs and used for non-invasive imaging in vivo, results that were supported by previous studies showing that XEOL emission wavelengths can be tuned by altering the NP composition, and through the changing emission wavelengths to enable the use ofdifferent drugs.[4,5] XEOL imaging is advantageous due to the lack of autofluorescence, excellent soft tissue penetration of X-ray in that is also has a visible emission within the biological window. Moreover, through encapsulation of the hydrophobic PpIX with a polymeric PGA-PEG coating, we quenched the radioluminescent signal from the XGP NPs. From these measurements of the radioluminescence peak ratio, we were able to observe the drug release

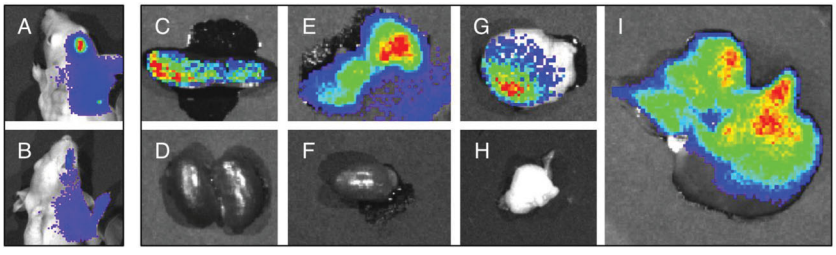

Figure 6. Athymic BALB/c mice implanted with intracranial U-138MG glioblastoma tumors were administered XGP through the tail vein. Radioluminescent imaging 24 h after the injection shows a strong XGP signal in the brain tumors: the non-invasive imaging of the XGP in tumors in both the (A) dorsal and (B) ventral aspect. Explanted tissues were also imaged to determine the biodistribution of XGP following injection. NPs were detected in organs of the reticuloendothelial system, and in the brain (tumor) and lungs: (C) spleen, (D) kidney, (E) lungs, (F) heart, (G) brain with tumor, (H) fat, (I) liver.

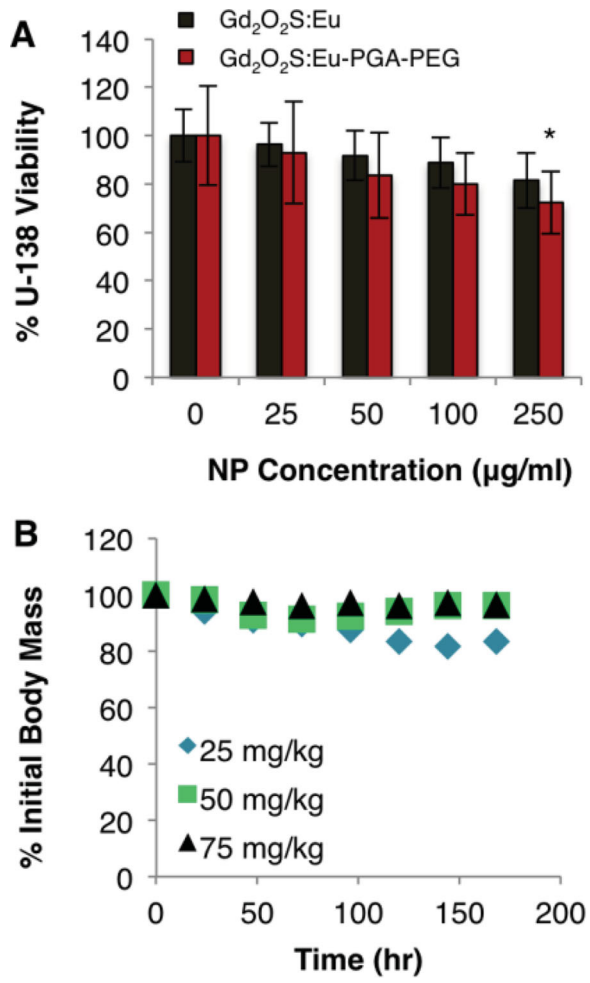

Figure 7. (A) Cytotoxicity of uncoated NPs and XGP in U-138MG. Samples were compared with a Tukey's HSD test, and * indicates statistically significant difference from the 0 μg/mL control. (B) Dose escalation study of XGP in BALB/c mice.

a removal kinetics. The polymer coating further served as an effective means for controlling drug release kinetics, and this drug encapsulation approach could be extended to other hydrophobic drugs. Both the polymer-coating composition and the content can be varied to precisely control the release kinetics, making polymer coated radioluminescent NPs a most versatile platform for theranostic applications. Our results also determined that drug release kinetics could be measured in U-138GBM cells. Finally, XGP was shown to be non-toxic in vitro at doses up to 100 μg/mL in U-138MG cells, and showed no significant adverse response in vivo at doses up to 75 mg/kg after intravenous injection into BALB/c mice. Although these results are most promising, more advanced toxicological studies are necessary to determine the maximum tolerated dose, the long-term fate, and potential long-term toxicity of XPG NPs. While further studies are also necessary to test the in vivo release, this research clearly demonstrates a robust approach for non-invasively measuring the release kinetics into cells.

4. Experimental Section

Materials: Gadolinium(III) nitrate, europium(III) nitrate, urea, glycerol, sodium fluoride, sulfur powder, ammonium hydroxyide, glycolide, tetraethyl orthosilicate (TEOS), (3-aminopropyl) triethoxysilane (APTES), and all solvents were purchased from Sigma-Aldrich. Poly(1-(2-oxo-1-pyrrolidinyl)ethylene) (PVP), MW = 40 kDa, was purchased from Spectrum Chemicals (New Brunswick, NJ). Methoxy-PEG-isocyanate, MW = 5 kDa, was purchased from Nanocs, Inc. (New York, NY).

Nanoparticle Characterization: FT-IR was performed with a Thermo-Nicolet Magna 550 equipped with a Thermo-SpectraTech Foundation series Endurance Diamond ATR. Thermogravimetric analysis was performed on a Hi-Res TGA 2950 thermogravimetric analyzer (TA Instruments, New Castle, DE) under nitrogen within a range of 25 °C to 600 °C at 20 °C/min. For the radioluminescence experiments, X-rays were generated by a mini X-ray tube (Amptek Inc, Bedford, MA, USA) operated at a tube voltage of 40 kV and a tube current of 99 μA. Radioluminescence measurements were taken by a DMI 5000M microscope (Leica, Wetzlar, Germany) equipped with a DNS 300 Spectrometer (Intevac-DeltaNu, Laramie, WY, USA) with a 150 lines/mm grating blazed at 500 nm and with a cooled iDUS-420BV CCD camera (Andor, South Windsor, CT, USA). In vivo radioluminescence images were captured with an IVIS Lumina-XR imaging system (Caliper Life Sciences, Hopkinton, MA, USA). Transmission electron microscope images were taken on a Hitachi H7600T at 115 kV.

Gd_2O_2S:Eu Nanoparticle Synthesis: Gadolinium(III) nitrate ($Gd(NO_3)_3$) was dissolved to a concentration of 1 M in 2 L distilled water (diH2O), and brought to 80 °C with stirring. Europium(III) nitrate ($Eu(NO_3)_3$) was added at a concentration of 200 mM. Urea (30 g, 0.49 mol) was added and stirred for 40 min. The reaction vessel was placed in an ice bath and cooled to room temperature. The nanoparticles were collected via centrifugation and washed with diH_2O, and then re-dispersed in a 20 mL diH_2O solution. Sodium fluoride (NaF) was dissolved at 1 mg/mL in diH_2O, and 4 mL of NaF was added, followed by the addition of 24 mL of glycerol to the nanoparticle solution within the vessel. The solution was heated to 120 °C under N_2 flow for 1 h, and the temperature was raised to 170 °C. After stirring for 1 h, the solution was cooled to room temperature and washed with diH_2O. The nanoparticles were re-dispersed in 200 ml diH_2O, sonicated, and the solution was brought to 80 °C and stirred. Next, PVP (1.2 g, 0.03 mmol), urea (4g, 0.07 mol), 1 mL of 1 M $Gd(NO_3)_3$ and 250 μL of 200 mM $Eu(NO_3)_3$ were added sequentially and stirred for 1 h. The solution was then cooled to room temperature and nanoparticles were first washed in diH_2O, and then ethanol. The nanoparticles were heated to 80 °C to dry, heated again for 2 h at 600 °C to remove impurities, and heated a third time to 700 °C under an argon flow with sulfur powder for another hour for sulfidation. They were then collected and cooled to room temperature.

Surface Functionalization and Polymer Coating of Gd_2O_2S:Eu Nanoparticles: Gd_2O_2S:Eu NPs (60 mg) were sonicated and suspended in 50 mL ethanol with 2 ml diH_2O, PVP (0.3 g, 0.0075 mmol), and ammonium hydroxide (2 mL). TEOS (20 μL, 0.089 mmol) was added to the solution after the solution was stirred for 10 min. The particles were stirred and aged at room temperature for two hours, at which point APTES (20 μL, 0.085 mmol) was added to the suspension and the reaction was stirred for 1 h. The resulting particles were separated by centrifugation and washed three times with ethanol. Nanoparticles were covalently coated with poly(glycolide) (PGA) using a room temperature, ring-opening polymerization. Prior to each reaction reagents were dried under vacuum at 32 inHg. In a typical reaction, Gd_2O_2S:Eu NP (40 mg) was dried with various amounts of glycolide was dissolved in organic solvent, and phosphazene base P_2-t-Bu was added as a catalyst. The reaction was continued under nitrogen. Next, methoxy-PEG-isocyanate was dissolved in 2 mL of acetonitrile and added directly to the reaction mixture, which was then continued under nitrogen and finally washed via centrifugation. The product was lyophilized and stored at –20 °C under nitrogen until further use.

In Vitro Uptake: U-138MG glioblastoma cells (ATCC, Manassas, VA, USA) were seeded at 1 million cells per T-25 flask. The next day, XGP particles were added at a concentration of 25 μg/mL and incubated for various time points. At each time point, the media was removed, the cells were gently washed twice with a sterile phosphate buffered saline (PBS), and fresh media was added. Triplicate flasks were analyzed for NP uptake at each time point. The cells were lifted with trypsin, collected by centrifugation at 1000 rpm for 5 min, and a supernatant was disposed. They were then re-suspended in 100 μL of sterile PBS, and the radioluminescence was measured using the IVIS Lumina-XR imaging system.

Drug Loading and Release Measurements: Measuring the effect of drug loading on the radioluminescent peak ratio was accomplished by dissolving PpIX at various concentrations in an 80/20 v/v% solution of acetonitrile and dimethyl sulfoxide. XGP was then dissolved in this drug solution at 5 mg/mL, and rotated for 1 h on a rotisserie protected from light. NP/drug solution was then dropped at a 1:2 ratio in H_2O and stirred for 2 h. The NPs were then washed as previously described, and radioluminescence measurements were taken immediately. The signal was measured by taking the average radioluminescent peak intensity at 630 nm, which was normalized with the average radioluminescent peak intensity at 700 nm, as PpIX does not absorb the 700 nm peak. For the drug release studies, XGP was loaded as described with PpIX at a concentration of 2 mg/mL. After stirring, XGP/PpIX samples were washed and re-dispersed in diH_2O at 25 mg/mL, and placed in the a 3.5 kD MWCO Slide-A-Lyzer MINI dialysis unit. The dialysis units were placed in 2 mL microcentrifuge tubes with diH_2O and stored at 37 °C. At each time point, the dialysate was exchanged with fresh diH_2O and measurements were taken via radioluminescence. The dialysate was lyophilized, reconstituted in dimethyl sulfoxide, and PpIX concentration was measured by a fluorescent plate reader (ex. 400 nm, em. 635 nm). In vitro measurement of drug release in U-138MG cells was performed by first seeding cells at one million cells per T-25 flask. XGP was loaded with PpIX at 2 mg/mL as previously described. XGP/PpIX was re-dispersed at 25 μg/mL in EMEM and added to cells for 24 h. After initial incubation, the cells were gently washed twice with sterile PBS and replenished with fresh EMEM. To measure the intracellular release at each time point, the cells were washed with PBS, and lysed via 3x freeze-thaw cycles (at 20 min per cycle). The cell debris and NPs were then pelleted via centrifugation at 2500 rpm for 5 min. The supernatant containing free PpIX was separated, lyophilized, reconstituted in dimethyl sulfoxide and quantitatively analyzed with a fluorescent plate reader. The cell debris and XGP were re-dispersed in 100 μL of sterile PBS and radioluminescent measurements were taken. Change in spectral ratio was determined as previously described. The cell debris was then lyophilized, reconstituted in dimethyl sulfoxide, and PpIX content was analyzed with a fluorescence plate reader. A Nikon Eclipse Ti was used for the confocal microscopy. Cells were seeded at 12 000 per chamber in a Lab-Tek 8-chambered slide. XGP was loaded with PpIX at 2 mg/mL as previously described, and re-dispersed in sterile EMEM at 100 μg/mL. XGP without PpIX was prepared as a control. Also, PpIX dispersed at 6 μM in EMEM was added to cells to verify that XGP improves PpIX uptake into cells. Both the control media, the PpIX within the media, the XGP without PpIX, and the XGP loaded with the PpIX were incubated with cells for 6 h. Subsequently, the cells were gently washed twice with sterile PBS and fresh media was added. The cells were incubated for a total of 24 h, and subsequently fixed with a 4% formaldehyde solution in PBS for 30 min. They were next incubated with a 0.1% Triton-X solution for 2 min, and actin was stained with Alexa Fluor 488 phalloidin. The chambers were removed and the cells were mounted with a VectaShield fluorescent mounting media containing DAPI.

In Vivo Biodistribution: All mice were housed at the Clemson University Godley-Snell Research Center, with all research conducted in accordance with Clemson University Institutional Animal Care and Use Committee (IACUC) approved protocols. For in vivo biodistribution studies, athymic nude BALB/c mice (Harlan) were implanted with intracranial tumors of U-138MG following the protocol of Ozawa et al.[32] Briefly, U-138MG cells were washed with sterile PBS, collected and concentrated in serum-free EMEM at 40 million cells/mL. 100 μL of cell suspension was added to 100 μL of Matrigel (Becton Dickinson). The mice were anesthetized with ketamine-xylazine, the skin was disinfected with chlorohexidine and the eyes were lubricated with PuraLube eye ointment. A 1 cm sagittal incision was made across the top of the skull, which was sterilized with hydrogen peroxide. A hole was made 2 mm anterior and 1 mm lateral to the bregma using a 25-gauge needle. Next, 3 μL of cell solution was slowly injected 3 mm deep into the brain over one minute. The skull was closed using dental cement and the incision site was stapled shut. The tumors were allowed to grow for 10 days, after which the biodistribution studies were performed. Radioluminescent NPs were prepared for injection by suspending at 5 mg/ml in acetonitrile. A single volume of NP solution was dropped into two volumes of sterile H_2O under a laminar flow hood, and stirred for 2 h. The nanoparticles were washed twice in sterile H_2O, and once in a sterile PBS in a 100 kD MWCO centrifugal filter unit. Next, 200 μL of NPs were administered via tail vein injection at concentrations of 1 mg/mL. The mice were euthanized 24 h after injection and radioluminescent images were taken of the head and abdomen on the dorsal and ventral aspects. The liver, spleen, kidney, lung, heart, brain, and fat were also imaged using radioluminescence.

In Vitro and In Vivo Toxicity: U-138MG cells were seeded at 10 000 cells/well in a black, clear-bottom, 96-well plate. Uncoated Gd_2O_2S:Eu-NH_2 NPs or XGP were prepared in acetonitrile and diH2O as previously described and added to cells at various concentrations. U-138MG were incubated with NPs for 24 h, and then washed gently with sterile PBS. Presto Blue cell viability reagent (Life Technologies) was mixed with EMEM at a 1:9 ratio, and 100 μL was added to each well. The cells were incubated with the Presto Blue working reagent for 45 min, and then fluorescent measurements were recorded with a fluorescent plate reader (ex. 560 nm, em. 590 nm). Each fluorescent measurement was normalized with the average fluorescence of untreated (e.g. only received cell culture media) wells to determine the percent cell viability. Five replicates were used per treatment group. To determine the in vivo toxicity, BALB/c mice were systemically administered XGP via tail vein injections at concentrations of 25, 50, and 75 mg/kg body mass, and the mice were observed over a one-week period to determine the presence of any mass loss.

Acknowledgements

This research was partially supported through NSF CAREER award CHE1255535 to FW, HC, and JNA. The authors wish to acknowledge Mrs. Kim Ivey for the use of the TGA and FTIR, Dr. Terri Bruce, supervisor of the Clemson Light Imaging Facility (CLIF) for the use of the confocal microscope, and Dr. John Parrish and Mr. Travis Pruitt of the Godley Snell Animal Facility for the use of the IVIS Lumina XR small animal imaging system and for assistance with the in vivo studies. Finally, the authors also wish to thank the staff of the Clemson Advanced Materials Center for the use of their electron microscope.

Received: March 24, 2014
Revised: May 7, 2014
Published online: July 22, 2014

[1] a) M. E. Caldorera-Moore, W. B. Liechty, N. A. Peppas, *Acc. Chem. Res.* **2011**, *44*, 1061; b) A. J. Cole, V. C. Yang, A. E. David, *Trend. Biotechnol.* **2011**, *29*, 323; c) S. M. Janib, A. S. Moses, J. A. MacKay, *Adv. Drug Deliv. Rev.* **2010**, *62*, 1052; d) T. Lammers, S. Aime, W. E. Hennink, G. Storm, F. Kiessling, *Acc. Chem. Res.* **2011**, *44*, 1029; e) T. Lammers, F. Kiessling, W. E. Hennink, G. Storm, *Mol. Pharm.* **2010**, *7*, 1899; f) R. Paulmurugan, B. Oronsky, C. F. Brouse, T. Reid, S. Knox, J. Scicinski, *Theranostics* **2013**, *3*, 437.

[2] a) C. K. Huang, C. L. Lo, H. H. Chen, G. H. Hsiue, *Adv. Funct. Mater.* **2007**, *17*, 2291; b) D. Kim, Y. Y. Jeong, S. Jon, *ACS Nano*

2010, *4*, 3689; c) F. Dilnawaz, A. Singh, C. Mohanty, S. K. Sahoo, *Biomaterials* **2010**, *31*, 3694.

[3] a) B. L. Viglianti, A. M. Ponce, C. R. Michelich, D. Yu, S. A. Abraham, L. Sanders, P. S. Yarmolenko, T. Schroeder, J. R. MacFall, D. P. Barboriak, O. M. Colvin, M. B. Bally, M. W. Dewhirst, *Magn. Reson. Med.* **2006**, *56*, 1011; b) S.-H. Hu, K.-T. Kuo, W.-L. Tung, D.-M. Liu, S.-Y. Chen, *Adv. Funct. Mater.* **2009**, *19*, 3396; c) T. Moore, H. Chen, R. Morrison, F. Wang, J. N. Anker, F. Alexis, *Mol. Pharm.* **2014**, *11*, 24; d) J. S. Basuki, H. T. T. Duong, A. Macmillan, R. B. Erlich, L. Esser, M. C. Akerfeldt, R. M. Whan, M. Kavallaris, C. Boyer, T. P. Davis, *ACS Nano* **2013**, *7*, 10175; e) B. Kang, M. M. Afifi, L. A. Austin, M. A. El-Sayed, *ACS Nano* **2013**, *7*, 7420; f) J. Tang, B. Kong, H. Wu, M. Xu, Y. Wang, Y. Wang, D. Zhao, G. Zheng, *Adv. Mater.* **2013**, *25*, 6569; g) Q. Xing, N. Li, D. Chen, W. Sha, Y. Jiao, X. Qi, Q. Xu, J. Lu, *J. Mater. Chem. B* **2014**, *2*, 1182; h) F. Alexis, J. N. Anker, *Therapeutic Deliv.* **2014**, *5*, 97.

[4] X. Kang, Z. Cheng, C. Li, D. Yang, M. Shang, P. Ä. Ma, G. Li, N. Liu, J. Lin, *J. Phys. Chem. C* **2011**, *115*, 15801.

[5] H. Chen, T. Moore, B. Qi, D. C. Colvin, E. K. Jelen, D. A. Hitchcock, J. He, O. T. Mefford, J. C. Gore, F. Alexis, J. N. Anker, *ACS Nano* **2013**, *7*, 1178.

[6] J. Lai, B. P. Shah, E. Garfunkel, K.-B. Lee, *ACS Nano* **2013**, *7*, 2741.

[7] a) P. M. Gullino, F. H. Grantham, S. H. Clark, *Cancer Res.* **1962**, *22*, 1031; b) J. R. Levick, *Q. J. Exp. Physiol.* **1987**, *72*, 409; c) B. P. Mahoney, N. Raghunand, B. Baggett, R. J. Gillies, *Biochem. Pharmacol.* **2003**, *66*, 1207; d) D. Fukumura, R. K. Jain, *J. Cell. Biochem.* **2007**, *101*, 937; e) Y. Hassid, E. Eyal, R. Margalit, E. Furman-Haran, H. Degani, *Microvascular Res.* **2008**, *76*, 94; f) R. K. Jain, T. Stylianopoulos, *Nat. Rev. Clin. Oncol.* **2010**, *7*, 653; g) B. Mattix, T. Moore, O. Uvarov, S. Pollard, L. O'Donnell, K. Park, D. Horne, J. Dhulekar, L. Reese, D. Nguyen, J. Kraveka, K. Burg, F. Alexis, *Nano LIFE* **2013**, *03*, 1343003.

[8] U. Prabhakar, H. Maeda, R. K. Jain, E. M. Sevick-Muraca, W. Zamboni, O. C. Farokhzad, S. T. Barry, A. Gabizon, P. Grodzinski, D. C. Blakey, *Cancer Res.* **2013**, *73*, 2412.

[9] a) D. Chen, S. Zhu, H. Yi, X. Zhang, D. Chen, J. Liang, J. Tian, *Med. Phys.* **2013**, *40*, 031111; b) H. Chen, D. C. Colvin, B. Qi, T. Moore, J. He, O. T. Mefford, F. Alexis, J. C. Gore, J. N. Anker, *J. Mater. Chem.* **2012**, *22*, 12802.

[10] G. Pratx, C. M. Carpenter, C. Sun, L. Xing, *IEEE Trans. Med. Imaging* **2010**, *29*, 1992.

[11] C. M. Carpenter, G. Pratx, C. Sun, L. Xing, *Phys. Med. Biol.* **2011**, *56*, 3487.

[12] a) J. Liu, F. Erogbogbo, K.-T. Yong, L. Ye, J. Liu, R. Hu, H. Chen, Y. Hu, Y. Yang, J. Yang, I. Roy, N. A. Karker, M. T. Swihart, P. N. Prasad, *ACS Nano* **2013**, *7*, 7303; b) G. Chen, J. Shen, T. Y. Ohulchanskyy, N. J. Patel, A. Kutikov, Z. Li, J. Song, R. K. Pandey, H. Ågren, P. N. Prasad, G. Han, *ACS Nano* **2012**, *6*, 8280.

[13] H. Chen, M. M. Rogalski, J. N. Anker, *Phys. Chem. Chem. Phys.* **2012**, *14*, 13469.

[14] a) C. Sun, G. Pratx, C. M. Carpenter, H. Liu, Z. Cheng, S. S. Gambhir, L. Xing, *Adv. Mater.* **2011**, *23*, H195; b) H. Chen, D. Sulejmanovic, T. Moore, D. C. Colvin, B. Qi, O. T. Mefford, J. C. Gore, F. Alexis, S.-J. Hwu, J. N. Anker, *Chem. Mater.* **2014**, *26*, 2105; c) H. Chen, B. Qi, T. Moore, F. Wang, D. C. Colvin, L. D. Sanjeewa, J. C. Gore, S.-J. Hwu, O. T. Mefford, F. Alexis, J. N. Anker, *Small* **2014**, doi: 10.1002/smll.201303769.

[15] a) H. Chen, D. E. Longfield, V. S. Varahagiri, K. T. Nguyen, A. L. Patrick, H. Qian, D. G. VanDerveer, J. N. Anker, *Analyst* **2011**, *136*, 3438; b) H. Chen, A. L. Patrick, Z. Yang, D. G. VanDerveer, J. N. Anker, *Anal. Chem.* **2011**, *83*, 5045.

[16] M. M. Moronne, *Ultramicroscopy* **1999**, *77*, 23.

[17] V. Bagalkot, L. Zhang, E. Levy-Nissenbaum, S. Jon, P. W. Kantoff, R. Langer, O. C. Farokhzad, *Nano Lett.* **2007**, *7*, 3065.

[18] a) Z. Xu, Y. Gao, S. Huang, P. Ma, J. Lin, J. Fang, *Dalton Trans.* **2011**, *40*, 4846; b) G. Tian, W. Ren, L. Yan, S. Jian, Z. Gu, L. Zhou, S. Jin, W. Yin, S. Li, Y. Zhao, *Small* **2013**, *9*, 1929.

[19] a) D. E. J. G. J. Dolmans, D. Fukumura, R. K. Jain, *Nat. Rev. Cancer* **2003**, *3*, 380; b) R. R. Allison, C. H. Sibata, *Photodiag. Photodyn. Ther.* **2010**, *7*, 61.

[20] a) F. Alexis, E. M. Pridgen, R. Langer, O. C. Farokhzad, *Handb. Exp. Pharmacol.* **2010**, 55; b) J.-H. Park, L. Gu, G. von Maltzahn, E. Ruoslahti, S. N. Bhatia, M. J. Sailor, *Nat. Mater.* **2009**, *8*, 331; c) A. I. Minchinton, I. F. Tannock, *Nat. Rev. Cancer* **2006**, *6*, 583.

[21] A. Juzeniene, T. T. Thu Tam, V. Iani, J. Moan, *Free Radic. Biol. Med.* **2009**, *47*, 1199.

[22] H. Koo, H. Lee, S. Lee, K. H. Min, M. S. Kim, D. S. Lee, Y. Choi, I. C. Kwon, K. Kim, S. Y. Jeong, *Chem. Comm.* **2010**, *46*, 5668.

[23] a) P. Juzenas, A. Juzeniene, O. Kaalhus, V. Iani, J. Moan, *Photochem. Photobiol. Sci.* **2002**, *1*, 745; b) P. A. Valdés, F. Leblond, V. L. Jacobs, B. C. Wilson, K. D. Paulsen, D. W. Roberts, *Sci. Rep.* **2012**, 2.

[24] G. A. Kumar, M. Pokhrel, A. Martinez, R. C. Dennis, I. L. Villegas, D. K. Sardar, *J. Alloys Compds.* **2012**, *513*, 559.

[25] B. H. Johnson, M. H. Hecht, *Nat. Biotechnol.* **1994**, *12*, 1357; b) D. Svec, D. Andersson, M. Pekny, R. Sjöback, M. Kubista, A. Ståhlberg, *Front. Oncol.* **2013**, *3*, 274.

[26] a) K. S. Soppimath, T. M. Aminabhavi, A. R. Kulkarni, W. E. Rudzinski, *J. Controlled Rel.* **2001**, *70*, 1; b) S. N. Rothstein, J. E. Kay, F. J. Schopfer, B. A. Freeman, S. R. Little, *Mol. Pharm.* **2012**, *9*, 3003.

[27] a) M. A. Perazella, *Clin. J. Am. Soc. Nephrol.* **2009**, *4*, 461; b) J. Perez-Rodriguez, S. Lai, B. D. Ehst, D. M. Fine, D. A. Bluemke, *Radiology* **2009**, *250*, 371.

[28] a) F. Alexis, E. Pridgen, L. K. Molnar, O. C. Farokhzad, *Mol. Pharm.* **2008**, *5*, 505; b) T. L. Moore, J. E. Pitzer, R. Podila, X. Wang, R. L. Lewis, S. W. Grimes, J. R. Wilson, E. Skjervold, J. M. Brown, A. Rao, F. Alexis, *Part. Part. Syst. Charact.* **2013**, *30*, 365.

[29] H. Aoki, H. Aoki, T. Kutsuno, W. Li, M. Niwa, *J. Mater. Sci.: Mater. Med.* **2000**, *11*, 67.

[30] a) G. F. Paciotti, L. Myer, D. Weinreich, D. Goia, N. Pavel, R. E. McLaughlin, L. Tamarkin, *Drug Deliv.* **2004**, *11*, 169; b) R. Goel, N. Shah, R. Visaria, G. F. Paciotti, J. C. Bischof, *Nanomedicine* **2009**, *4*, 401; c) S. K. Libutti, G. F. Paciotti, A. A. Byrnes, H. R. Alexander, W. E. Gannon, M. Walker, G. D. Seidel, N. Yuldasheva, L. Tamarkin, *Clin. Cancer Res.* **2010**, *16*, 6139.

[31] a) T. K. Jain, M. K. Reddy, M. A. Morales, D. L. Leslie-Pelecky, V. Labhasetwar, *Mol. Pharm.* **2008**, *5*, 316; b) R. Weissleder, D. D. Stark, B. L. Engelstad, B. R. Bacon, C. C. Compton, D. L. White, P. Jacobs, J. Lewis, *Am. J. Roentgenol.* **1989**, *152*, 167.

[32] T. Ozawa, C. D. James, *J. Vis. Exp.* **2010**, *41*, e1986.